Available online at www.sciencedirect.com

ScienceDirect

journal homepage: www.elsevier.com/locate/issn/15375110

Special Issue: Robotic Agriculture

Research Paper

Close-range air-assisted precision spot-spraying for robotic applications: Aerodynamics and spray coverage analysis

Aleš Malneršič [a,*], Matevž Dular [a], Brane Širok [a], Roberto Oberti [b], Marko Hočevar [a]

[a] University of Ljubljana, Faculty of Mechanical Engineering, Aškerčeva 6, SI 1000 Ljubljana, Slovenia
[b] University of Milan, Department of Agricultural and Environmental Sciences, Celoria 2, 20133 Milano, Italy

ARTICLE INFO

Article history:
Published online 25 January 2016

Keywords:
Precision spraying
Agricultural robotics
Airflow
Plant motion
Movement of leaves
Spray deposition

Orchards and grapevines are currently sprayed overall. Most bush and tree crop sprayers use airflow assistance which generates movements in canopy exposing both sides of the leaves to the spray. Also, large coherent vortices are formed further contributing to improved spray coverage. A new close-range air-assisted spot-spraying method for the selective treatments of disease foci is evaluated here which is promising for reduction of pesticides. Targets structures are expected to have typical diameters around 150 mm and the size of the unit matches this. In contrast to conventional methods, this size of unit prevents the generation of large scale coherent turbulent structures in the airflow that could provide spray coverage of both sides of the target leaves. Therefore, to enhance the beneficial effects of local turbulence, and to induce leaf movement whilst retaining the small size of the spray unit, a rotating screen to generate airflow pulses with discrete peaks in velocity was added and tested. Experiments on the close-range spraying of young grapevine plants using the rotating airflow screen were performed. A high-speed camera, image analysis system and water sensitive papers were used for analysis of the spraying. Natural frequencies of individual leaves showed sharp fluctuations at discrete frequencies and single leaf fluctuations of root mean square velocity corresponded well to the pulsating airflow. Spraying was evaluated as percentage spray coverage and number of droplet impacts. Spray coverage of front side of leaves (facing the sprayer) was good, but coverage on the back of the leaves was limited.

* *Corresponding author.*
E-mail addresses: ales.malnersic@fs.uni-lj.si (A. Malneršič), matevz.dular@fs.uni-lj.si (M. Dular), brane.sirok@fs.uni-lj.si (B. Širok), roberto.oberti@unimi.it (R. Oberti), marko.hocevar@fs.uni-lj.si (M. Hočevar).
http://dx.doi.org/10.1016/j.biosystemseng.2016.01.001
1537-5110/

Nomenclature

Abbreviations

CROPS	Clever Robots for Crops
RMS	Root Mean Square
SEEF	Spraying End Effector
WSP	Water Sensitive Paper

Symbols

C(i,j)	correlation at position (i,j)
$\bar{f}$	average value of grey level of all points in the image f
f(x,y)	image at position (x,y)
K	width of sub image w (pixel)
L	height of sub image w (pixel)
M	width of image f (pixel)
N	height of image f (pixel)
N	number of measurements
R	normalised correlation coefficient
Tu	turbulence level %
U_i	airflow velocity (m s^{-1})
U_{mean}	mean airflow velocity (m s^{-1})
U_{RMS}	root mean square of airflow velocity (m s^{-1})
$\overline{w}$	average value of grey level of all points in the sub image w
w(x,y)	sub image at position (x,y)

1. Introduction

Application of agrochemicals is at present the method most used to protect plants from diseases, pests and weeds (Oerke & Dehne, 2004). To do this, pesticide formulations are diluted in water and distributed over the vegetation in form of sprays. To protect plants from diseases and pests, agrochemicals are sprayed uniformly to ensure coverage of susceptible targets at the appropriate time in the season. In orchards, grapevines and greenhouses susceptible targets (fruits, bunches, new sprouts, younger leaves, etc.) can be located anywhere in the vegetation, consequently current spraying techniques aims to cover all parts of plants, front and behind, top and bottom, as well as within the canopy.

As a result, high volume air-flow has been used to assist the transport and deposition of pesticide droplets the innermost parts of the canopy. Coarse spray can runoff from leaf surface or fail to deposit before reaching the target, whilst buoyancy can cause fine spray to drift away from target, with uncontrolled diffusion to soil and air. When treating plants with sparse canopy, a portion of the spray can travel through the foliage without being impacted. Thus a certain amount of pesticide can go off-target, with significant negative effects on production costs, impact on the environment and the quality of the produce (Cunha, Chueca, Garcerà, & Moltò, 2012; Jong, Snoo, & van de Zande, 2008; Otto et al., 2013).

Current robotic technologies can be applied to crop protection (Mulla, 2013) enabling the possibility of precise and selective targeting of the spray (Esau et al., 2014; Khot et al., 2012; Zamana et al., 2011). This represents one of the most promising options for reducing the amount of pesticide used, whilst maintaining crop-protection efficiency.

The concept of precise application of pesticides also involves the possibility of real-time adjustments of spraying application to the local needs of the target (plant, or part of the plant) on which the treatment is being applied (Andújar, Weis, & Gerhards, 2012; West et al., 2003). Hence, there is a need to develop and introduce techniques and systems for disease detection and pesticide distribution (Dekeyser et al., 2013) which are able to optimise the spot-application of pesticides according to the specific characteristics of the target, such as disease susceptibility, or the presence of infection symptoms.

In the broad field of agricultural robotics, research work is focused on the development and validation of intelligent and selective agricultural robots with crops-care capabilities by integrated use of cutting-edge robotics and further advancing of sensing technologies (Bontsema et al., 2014). Among these robots, a novel robotic sprayer may have a modular architecture, enabling flexible, adaptive and coordinated operation of multiple spraying units, giving to the machine the unprecedented capabilities of continuously adapting pesticide spraying pattern to the crop-canopy characteristics (as volume and foliage density), as well as selectively spot spraying only selected targets (as disease foci or fruits to be protected) (Oberti, Marchi, Tirelli, Calcante, Iriti, Borghese, 2014; Oberti, Marchi, Tirelli, Calcante, Iriti, Hočevar, et al., 2014). Rapid optical detection of disease is essential for precision spraying (West et al., 2003).

Here a new technique of spraying is introduced. For close range precision spraying small patches of disease are required to be treated during their early development. For this a close range precision application a spraying end effector (SEEF) is required. In the following an SEEF design will be presented and measurements of the properties of the airflow around the plant will be investigated. The compatibility of close range precision spraying with emerging robotic technology as part of the development of precision agriculture will be investigated.

1.1. *Flow aerodynamics around plants and leaves*

In the context of spraying tree and bush crops, airflow from an air-assisted sprayer carries pesticide spray towards its target and provides pressure to the surface of leaves and branches. The main goal is to establish flow conditions in canopies, required for good pesticide application (Endalew et al., 2010).

Large coherent structures can form under such flow conditions, enabling good penetration of the spray and interaction with the plant. These structures manifest themselves as airflow with constantly changing velocity and direction. To some extent, large coherent structures are responsible for flux of pesticide droplets to the backs of leaves (Sánchez-Hermosilla, Rincón, Páez, & Fernández, 2012) but plant movement also increases the probability of spray droplets impacting these areas (Pujol, Casamitjana, Serra, & Colomer, 2013).

To be effective against early discrete disease foci, and not causing excessive pesticide consumption, the size of the spray plume should be approximately of the same size as the disease foci. For close-range precision spot spraying of an

infected grapevine leaves the size of coherent structures should be around 150 mm in diameter (Ash, 2000). However, compared to conventional spraying, this size is too small to effectively disperse spray around plant leaves and deposit it on rear surfaces. Also, plant motion is limited by the size of leaves; at best small branches and individual leaves may be exposed to the SEEF airflow. Displacement and rotation of leaves, sprayed with SEEF, is likely to be more limited in compared with conventional spraying.

2. Close-range spraying end effector (SEEF)

The SEEF was designed such that pesticide could be locally applied to the position of the disease foci. The SEEF consisted of the following components: an airflow generator (axial fan), an airflow nozzle, a pesticide nozzle, a pesticide pump, electrical connections for power supply and control signals, a pesticide connection and a chassis. A schematic diagram of the SEEF is shown in Fig. 1.

2.1. SEEF design

The SEEF was designed to enable connection to robotic agricultural systems, such that developed under CROPS EU project (Bontsema et al., 2014). The SEEF was of lightweight construction since it was intended for installation on robotic arms.

A voltage regulator was used for regulation of rotational speed of axial fan. Air flow velocity at target distance from 0.3 m to 1.2 m was adjustable from 5 m s^{-1} to 15 m s^{-1}.

Airflow was generated by a 119 mm 90 W axial fan (4118 N/2H7P, Ebmpapst, Mulfingen, Germany). The tangential component of the airflow was transformed to an axial direction with flow straightener with inlet angle 19.5°. The diameter of the aerodynamic diffuser varied from 116 mm to 80 mm, an angle of 9.5° and length 120 mm.

Pesticide was supplied to the unit by a diaphragm pump (Shurflo 8000, PENTAIR, Worsley, UK) which was located with the pesticide reservoir in a control box outside the SEEF. The pesticide nozzle used was a full cone type with 30° flow angle (Type S 0.5 30°, Steinen, Parsippany, NJ, USA). The normal operating pressure of the circuit was 360 kPa. The pesticide volume flow rate at selected pressure was 1.0 l min^{-1} which was turned on/off and regulated by an electromagnetic valve.

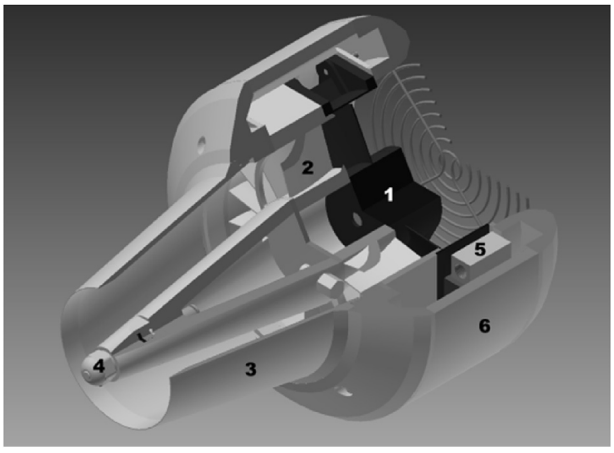

Fig. 1 – Close range spraying end effector. 1. Axial fan, 2. Flow straightener, 3. Airflow diffuser, 4. Pesticide nozzle, 5. Pesticide valve, 6. SEEF case with voltage regulator and pesticide nozzle switch.

2.2. Airflow structure

The airflow at the exit from aerodynamic nozzle of SEEF should contain only small tangential and radial velocity components since both components cause expansion of the airflow with the increasing distance from the SEEF. Unwanted expansion of the airflow prevents spot spraying of diseased plant parts occurring particularly for targets located far away from the SEEF and deep within the canopy. To reduce airflow expansion, the SEEF was equipped with flow straightener and a conical aerodynamic nozzle as described in Section 2. However, the use of a flow straightener and conical aerodynamic nozzle reduce turbulence in the airflow and prevents the formation of large coherent structures. Lack of large coherent structures decreases probability of spray depositing on the back of leaves.

In general, large coherent structures feature low frequencies, while small coherent structures feature high frequencies. Large coherent structures, with their low frequency can coincide with the natural frequencies of branches and leaves and may produce increased plant movement causing the back of leaves to be exposed to spray.

As a possible remedy to the expected limited deposition on the back of leaves, pulsations in the airflow were deliberately introduced via a rotating screen. The rotating screen operated as a device that alternately stopped and allowed the airflow to pass through. Such arrangement was considered able to produce high airflow pulsations without significantly expanding the spray plume. Measurements of the airflow from the SEEF using the rotating screen are presented in the next section.

3. Measurement and analysis methods

Three measurement techniques were used to evaluate the operation of the SEEF: (1) aerodynamics measurements using hot-wire anemometry, (2) spray coverage and determination of the number of spray impacts using by water sensitive papers and (3) measurement the motion of plants and leaves using high speed imaging and analysis. They are described more in detail in the following subsections.

Pulsations of the airflow were achieved using a rotating circular airflow screen with four unevenly distributed openings. The diameter of each opening was 80 mm and the airflow screen was rotated by an electric motor, driven by a variable frequency drive.

3.1. SEEF aerodynamic measurements

To establish aerodynamic properties of the SEEF, instantaneous velocity measurements were performed using hot-wire anemometry. The experimental setup for measurement of

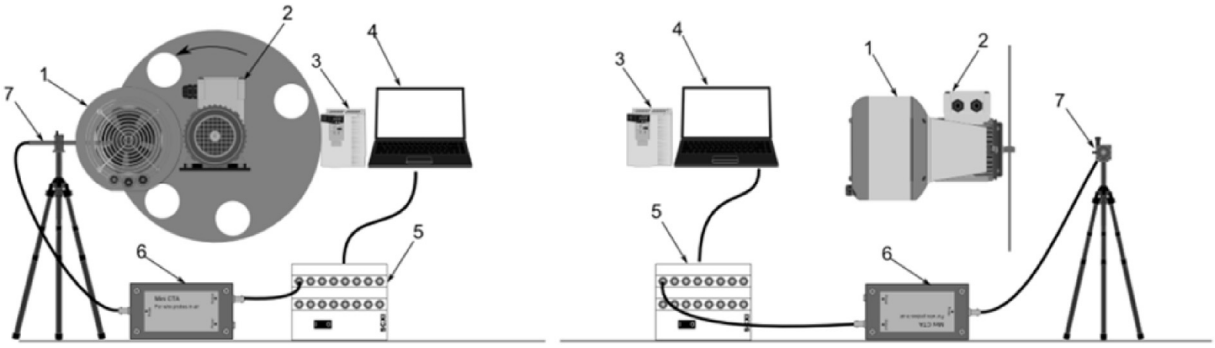

Fig. 2 – Measurement setup for SEEF airflow properties measurements with hot-wire anemometry, left: Rear view, right: Right side view; (1) SEEF, (2) electric motor with rotating airflow screen, (3) electric motor variable drive, (4) personal computer with multifunctional data acquisition board, (5) signal conditioner, (6) constant temperature anemometer and (7) hot wire sensor.

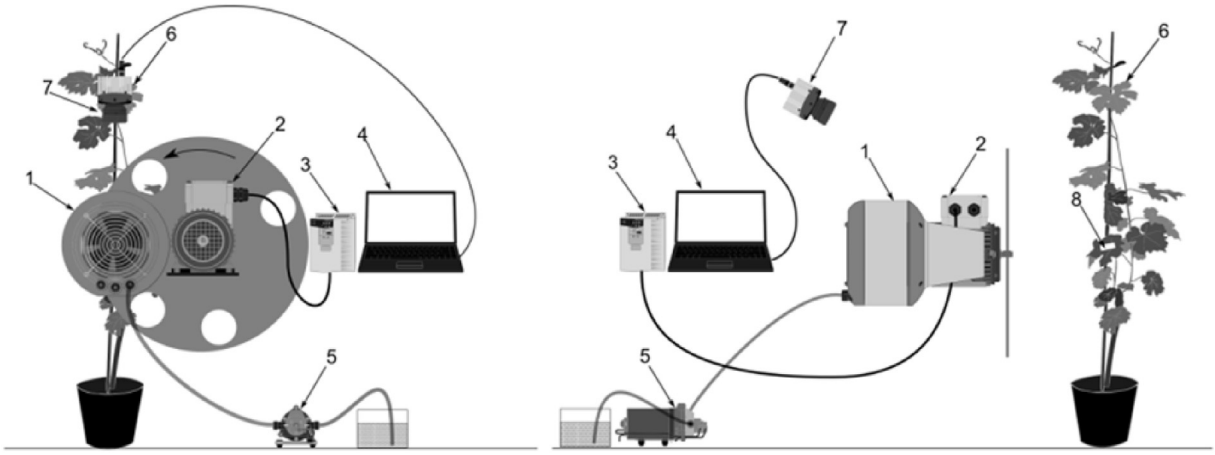

Fig. 3 – Measurement setup for plant and leaves motion analysis, left: Rear view, right: Right side view; (1) SEEF, (2) electric motor with rotating airflow screen, (3) electric motor variable drive, (4) personal computer, (5) pesticide pump, (6) plant, (7) high speed camera with lens and (8) water sensitive papers.

SEEF airflow properties is shown in Fig. 2. A hot wire anemometer (Mini CTA, Dantec, Denmark) with straight single wire sensor (55P11, Dantec, Skovlunde, Denmark) was used. The sensor wire diameter was 5 μm and length was 1.25 mm. Signal conditioning was performed using a 10 kHz Bessel filtering with an AC powered chassis (SCXI 1000, National Instruments Corp., Austin, TX, USA), an 8-channel isolation amplifier (SCXI-1120, National Instruments Corp.) and a BNC connection box (SCXI-1305, National Instruments Corp.). Data acquisition unit used a 16 bit A/D measurement board (NI 6212, National Instruments Corp.). Sampling frequency was 20 kHz and sampling interval was 10 s. Calibration and measurement were carried out according to procedure of Bruun (1995) and Jørgensen (2002). For measurement of flow temperature, a 4 wire Pt100 type A temperature sensor and a data acquisition unit (Agilent 34970A, Agilent technologies, Santa Clara, CA, USA) were used.

During measurements of aerodynamic flow properties SEEF spray nozzle was not operated. The SEEF was located at the same height and axis as hot wire anemometer probe and the probe was mounted with its hot-wire perpendicular to the direction of the main flow. The distance between SEEF nozzle and the hot-wire anemometer probe varied according to different operation points as shown in Table 1, being 0.7 m, 0.5 m and 0.3 m. Mean airflow velocity U_{mean}, root mean square (RMS) airflow velocity U_{RMS} and turbulence level T_u were calculated from the measurements according to guidelines in Jørgensen (2002). The RMS velocity was used as a measure for

Table 1 – Selection of operational-set points.

Operational set-point	Repetitions	Distance [m]	Air velocity at the location of target [ms^{-1}]	Pulsation frequency [Hz]	Spray
1	2	0.3	6.1	1.2	Yes
2	3	0.5	7.5	2	Yes
3	1	0.7	7.5	2	No

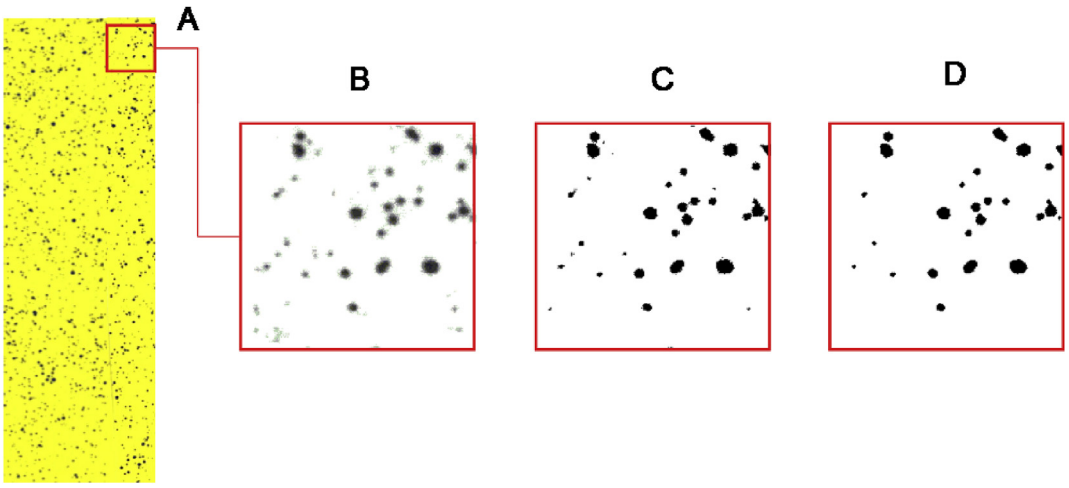

Fig. 4 – From the RGB image (A) the green channel of the WSP image was extracted (B) a sharp bimodal distribution of pixels grey levels was obtained which corresponded to the sensitive paper background and adsorbed droplets respectively. Given the fixed settings of the digital scanner, a constant threshold value (170 from 255) was applied to segment droplets pixels (C) and filtered with a morphological operation to remove noise pixels (D). (For interpretation of the references to colour in this figure legend, the reader is referred to the web version of this article.)

leaf velocity fluctuations, since the average velocity of leaves is zero, because leaves are attached to the plant.

Mean airflow velocity:

$$U_{mean} = \frac{1}{N}\sum_{1}^{N} U_i \quad (1)$$

Airflow velocity root mean square (RMS) (Jørgensen, 2002):

$$U_{RMS} = \left(\frac{1}{N-1}\sum_{1}^{N}(U_i - U_{mean})^2\right)^{0.5} \quad (2)$$

$$\text{Turbulence level}: \quad T_u = \frac{U_{RMS}}{U_{mean}} \quad (3)$$

Where U_i is airflow velocity and N is number of measurements.

3.2. *Spray coverage and number of impacts*

Within the grapevine (*Vitis vinifera* L.), two positions on both sides of the leaves were selected for an analysis of spray coverage and deposition as shown in Fig. 3. To analyse spray deposit water sensitive papers (WSP, Quantifoil Instruments GmbH, Jena, Germany) of size 75 mm × 26 mm were attached to the plants. The number of spray droplet spots and the percentage of coverage were evaluated for each WSP. Spray deposit and coverage of the droplets from different sprayings was quantified using WSP analysis. For each analysis, WSP were placed at equivalent places (Porras-Soriano, Porras-Piedra, & Soriano-Martn, 2005) and were attached to the selected leaves on both surfaces at fixed positions. They were collected approximately 10 min after they were completely dry. Spot-spraying time was set to 1 s, corresponding to a realistic application time and spraying was carried out using mains water. Measurements were performed indoors in a laboratory. Air temperature during measurements was 22 °C and relative humidity was around 50%.

After each experiment, the plant was allowed to dry completely and the WSPs were carefully detached and stored in sealed labelled plastic bags for subsequent imaging. Colour digital images of WSPs were acquired using a digital scanner at 1200 dpi, resulting in a nominal resolution of 21 μm pixel^{-1}.

The obtained RGB images were processed by custom software written in Matlab (R2013a, the MathWorks Inc., Natick, MA, USA) to obtain quantitative descriptors of spray deposit on the target. To this aim, the green channel of the WSP image was extracted (B, Fig. 4) obtaining a sharply bimodal distribution of grey levels, corresponding to background pixels (very high grey levels) and droplet trace pixels (very low grey levels) respectively.

Given the constant settings of the digital scanner, a constant threshold value (170 on 255) was applied to segment droplet pixels from their background in all the WSPs collected in the experiments (C, Fig. 4).

The obtained binary image was then filtered with a morphological opening operator (D, Fig. 4) to remove noise pixels from background and from the border of droplet regions. The resulting nominal resolution of images was then degraded to 42 × 42 μm^2

The pixel regions retained after the processing (D, Fig. 4) were then assumed to correspond to spray deposit on the WSP. By determining their quantity, dimensions, and spatial distribution, it was possible to characterise the spray deposit on the target.

For example, the red squared frame in Fig. 4A resulted to be spray droplets covering 3.7% of its area, with an average number of impacts of 62 drops cm^{-2}. The droplet population had a volume median diameter of 241 μm.

3.3. *Plant and leaves motion analysis by image analysis*

The camera used for image acquisition of plant motion was Fastec Hispec 4 (Fastec Imaging Corp., San Diego, CA, USA).

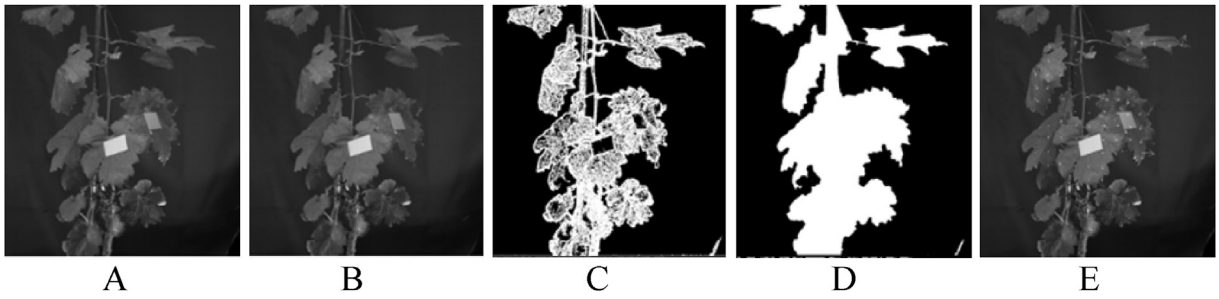

Fig. 5 – Sample analysis of plant leaves velocity. (A) first image of the image pair. (B) second image of the image pair, (C) first image after edge detection, (D) first image with closed holes, (E) velocity vectors overlaid over the first image of the image pair.

The camera operated at a resolution 800 × 858 pixel at 150 frames s^{-1} and was positioned above and slightly behind the SEEF. The number of acquired images in each series was 5000. A Nikkor 50 mm f/1.2 lens (Nikon, Tokyo, Japan) was used with the camera. A dark background was used for easier separation of the plant from the background. The plant was illuminated from two sides with 4 LED lights Cree XM-L T5 (Cree Inc., Durham, NC, USA) in a row that were 25 mm apart, placed on each side at distance 0.8 m between them and 0.5 m from the plant. LED lights were powered by a DC current source to ensure the continuous illumination.

During visualisation, leaves were spatially variable illuminated or screened by neighbouring leaves. Simple general or local intensity thresholding was inadequate to separate plant from the background. A combination of edge detection and morphology operations (Fig. 5) was therefore selected. Custom software program for image analysis was used, which was written in LabVIEW (National Instruments Corp.) using the Vision Development Module library.

Edge detection was performed using Sobel filtering method followed by outlying particle removal using erosion algorithm (Fig. 5C). For erosion, all objects in image were kept that were resistant to the specified number of erosions. Kept objects were rendered to the shape and size the same as before erosion algorithm. Best results were achieved using two consecutive erosions. After particle removal algorithm, holes were filled as shown in Fig. 5D.

A normalised cross correlation method was used for matching of patterns for displacement evaluation on series of images. Leaves are objects that change shape, rotation and to some extent also size, when they move in the spray plume both closer and further away from the camera.

A sub image $w(x,y)$ of size $K \times L$, is located inside image $f(x,y)$ of size $M \times N$. Here $K \leq M$ and $L \leq N$ (Fig. 6). Correlation among $w(x,y)$ and $f(x,y)$ in location (i, j) is given by the equation

$$C(i,j) = \sum_{x=0}^{L-1} \sum_{y=0}^{K-1} w(x,y) f(x+i, y+j) \tag{4}$$

where $i = 0,1 \ldots M-1$
$j = 0,1 \ldots N-1$,

The summation is in the region, where images w and f overlap. Sub image w moves over entire image and C is calculated according to Eq. (4) for every point in the image. The highest value of function C in the image denotes place, where sub image w corresponds the most to the image f.

The correlation method is susceptible to changes in image grey level (illumination) in the image f and sub image w. Therefore the normalised correlation coefficient R was used according to the equation

$$R(i,j) = \frac{\sum_{x=0}^{L-1}\sum_{y=0}^{K-1}(w(x,y)-\overline{w})\left(f(x+i,y+j)-\overline{f}(i,j)\right)}{\left[\sum_{x=0}^{L-1}\sum_{y=0}^{K-1}(w(x,y)-\overline{w})^2\right]^{\frac{1}{2}}\left[\sum_{x=0}^{L-1}\sum_{y=0}^{K-1}(f(x+i,y+j)-f(i,j))^2\right]^{\frac{1}{2}}} \tag{5}$$

Here $\overline{w}$ is average value of grey level of all points in sub image w and $\overline{f}$ is average value of f in the image. Value of R is in the interval from −1 and 1 and is independent of change of illumination of f and w.

Displacement estimation was performed in a selected matrix of locations. A template of selected size was extracted from the first image for every selected location. The template size 45 × 45 pixels was used. Among the locations in the second image, the one with the highest similarity was

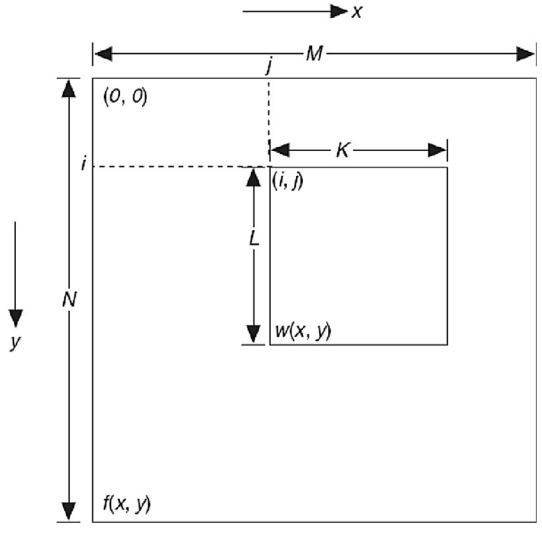

Fig. 6 – Principle of cross correlation displacement measurement.

considered where the distance from the template was smaller than a selected value. The lowest allowed similarity limit was selected to reject locations with poor matching. Subpixel accuracy and shift invariant search were performed, meaning that in a selected position of the search the template was not rotated.

From displacements and time difference, when two consecutive images were recorded, velocities in *x* and *y* direction were calculated (Fig. 5E).

3.4. *Operational set-points for spray coverage and number of impacts measurements*

Several operating conditions were explored during the experiments for measurements of spray coverage, number of impacts and plant and leaves motion with high speed imaging as shown in Table 1. Spraying and imaging was done simultaneously. In operational set-point 1 spraying was carried out twice on different plants and in operational set-point 2 spraying was carried out three times.

4. Results and discussion

The results of aerodynamic operation of SEEF are presented in Section 4.1, the results of the spraying with SEEF in Section 4.2 and the results of measurements of plant movement are presented in Section 4.3.

4.1. *Results of aerodynamic measurements*

Fig. 7 shows the decrease of axial velocity with increasing distance from the SEEF. Velocity is presented for the two settings of the fan rotational speed, one producing airflow with an average velocity of 10 m s^{-1} and the other 7.5 m s^{-1} both measured at a distance of 0.3 m from the SEEF.

Measurements of aerodynamic properties of SEEF were performed in the absence of the plant according to experimental setup shown in Fig. 2. Results are shown as turbulence levels and spectra of velocity fluctuations. Figure 8 shows power spectrum of velocity fluctuations for all selected operational-set points. Experimental results show that number of discrete peaks in velocity fluctuations decreases with

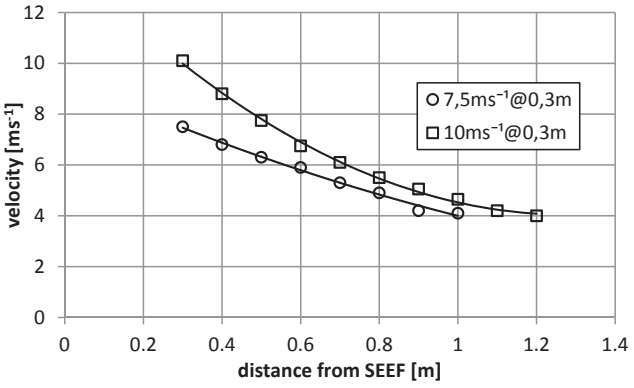

Fig. 7 – Relationship between distance from SEEF and airflow axial velocity.

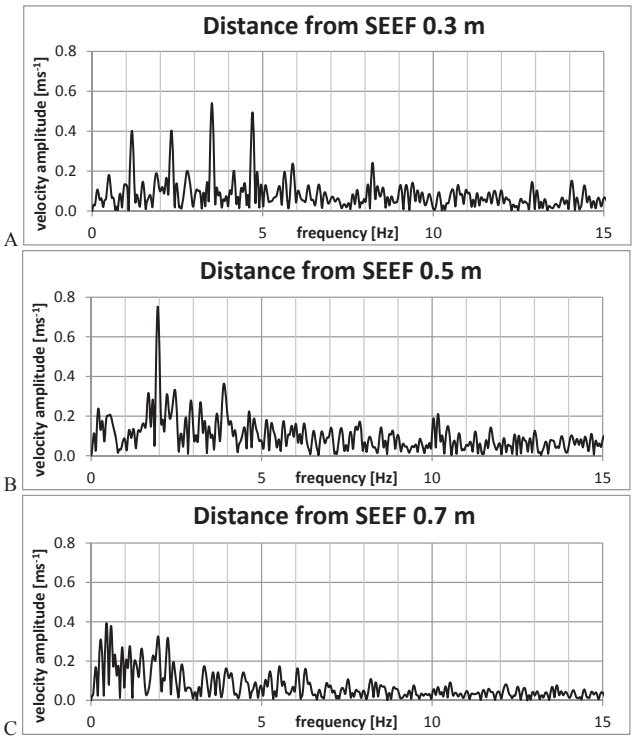

Fig. 8 – Airflow velocity power spectrum at location of the target at distances (A) 0.3 m, (B) 0.5 m and (C) 0.7 m from the SEEF.

distance of the measurement location from SEEF, number of discrete peaks in velocity fluctuations being the highest for operational-set points 1 (Fig. 8A, distance 0.3 m), and the lowest in operational-set point 3 (Fig. 8C, distance 0.7 m).

Selection of rotating screen with four unevenly distributed openings resulted in generation of the airflow with several independent frequency peaks of velocity fluctuations. In the operational-set point 1, four highest peaks of velocity fluctuations are at frequencies 1.2 Hz, 2.4 Hz, 3.5 Hz and 4.7 Hz. In the operational-set point 2 one high peak of velocity fluctuations is at frequency 2 Hz.

The airflow from the SEEF without the rotating screen contains only limited flow fluctuations. Since the generation of large velocity fluctuations and associated coherent structures occurs at the location of the rotating screen, then with increasing distance from the SEEF the discrete structures decay and a more coherent airflow occurs. At greater distances from SEEF (operational-set point 3), discrete peaks of velocity fluctuations are not discernible.

Turbulence levels are shown in Table 2. Turbulence levels in the case of operational-set point 1 (distance 0.3 m) were 66%, while in the case of operational-set point 2 (distance 0.5 m) turbulence levels were 52% and in operational-set point 3 (distance 0.7 m) turbulence level was 67%.

4.2. *Results of spray coverage and number of impacts measurements*

The selection of operational set-points to achieve good spray coverage and the maximum number of impacts (droplets

Table 2 – Integral parameters of spraying. In the first column of the table, right front of the leaf, the WSP was almost saturated and droplet images were not distinct.

Operational - set point	Repetition	Average leaf velocity [m s^{-1}]	Leaf RMS velocity [m s^{-1}]	Turbu lence level [%]	Spray coverage front side [%]		Spray coverage back side [%]		Droplet density [drops cm^{-2}]		Droplet density [drops cm^{-2}]	
					Left	Right	Left	Right	Left	Right	Left	Right
1	1	0.029	0.346	66	48.8	94.4	0.2	0.2	138	n.a.	8	7
	2	0.0052	0.243		31.5	13.9	9.5	2.1	133	177	118	61
2	1	0.0058	0.168	52	42.8	27.0	0.5	0.7	157	218	23	38
	2	0.0073	0.193		50.7	39.6	0.7	0.2	130	190	39	10
	3	0.0014	0.157		16.9	53.4	0.3	0.4	190	99	14	28
3	1	0.028	0.328	67								

cm^{-2}) is shown in Subsection 3.4. Figure 9 shows an effective spray diameter around 150 mm at distance 0.3 m and air velocity 7.5 m s^{-1}. Results of coverage and droplet density are shown in Table 2. Droplet density on front side of the leaves was good. At the operational-set point 1 and repetition 1, spray coverage on the right leaf was excessive (94.4%) and the spray droplets were not distinct. The Syngenta (2002) set lower limit for droplet density and in addition an interval of acceptable droplet densities. According to Syngenta (2002) and Cunha, Carvalho, and Marcal (2012), the minimum droplet density in the target area should be no less than 20 to 30 droplets cm^{-2} for insecticide or pre-emergence herbicide applications, 30 to 40 droplets cm^{-2} for contact post-emergence herbicides, and 50 to 70 droplets cm^{-2} for fungicide applications. For spray droplet volume median diameter 200 μm Syngenta (2002) set the range of acceptable droplet densities from 129 drops cm^{-2} to 258 drops cm^{-2}.

In this case the droplet density on the back of the leaves was <40 droplets cm^{-2} except at the operational-set point 1 and repetition 2, where on one back side of the leaf the droplet density reached 118 droplets cm^{-2} whilst on the other it was 61 droplets cm^{-2}. This is around or below the minimum droplet density in the target area (Syngenta, 2002) and less than the acceptable densities of droplet impacts (Syngenta, 2002). The spray droplet volume median diameter was 167 μm with standard deviation 40 μm.

Limited movement of the plant leaves, combined with small turbulent structures in the airflow, essentially prohibited spray being deposited on both sides of leaves. As a result, when spraying by SEEF, only front sides of the leaves were sprayed.

4.3. *Results of plant and leaves motion analysis by image analysis*

Introduction to image analysis procedure used was provided in Subsection 3.3. Average leaf velocity for the entire plant was calculated for each operation point as an average of all measured velocities on all images. Similarly leaf RMS velocity was calculated as a RMS of all measured velocities on all images.

Fig. 9 – Effective spray diameter at distance 0.3 m and air velocity 7.5 m s^{-1} shown by water sensitive paper.

Average RMS velocity vectors are overlaid on representing image for each operation point (Fig. 8). Velocity vectors are shown in red colour. Intensity of the colour represents percent of successfully calculated velocities at certain point. The origin of the coordinate system was in the top left corner of the domain. Since the RMS values of velocity fluctuations were always positive and velocity vectors were calculated as a RMS value of individual velocities of the complete sequence the vectors always points down and to the right. Using this visualisation method only velocities in x and y directions can be measured so velocity information about depth (z direction) is not available.

Average leaf velocity is close to zero, because leaves fluctuate around their equilibrium position. Leaf RMS velocity plots feature two distinctive intervals of velocities that correspond to two distances between SEEF and the plant. In the case of operational-set point 1 (distance 0.3 m) the RMS displacement was larger than for operational-set point 2 (distance 0.5 cm).

Leaf RMS velocity of fluctuations corresponded well with airflow turbulence levels for all operational-set points. In the case of operational-set point 2 (turbulence level 52%) leaf RMS velocity was from 0.157 m s^{-1} to 0.193 m s^{-1}. In the case of operational-set point 1 (turbulence level 66%) leaf RMS velocity was 0.243 m s^{-1} and 0.346 m s^{-1}.

Figure 11 shows frequency of fluctuations of leaves for operational-set point 3, repetition 1, left leaf, operational-set point 2, repetition 2, left leaf and operational-set point 1, repetition 2, left leaf. The frequency of fluctuations of leaves had narrow peaks of fluctuations around discrete frequencies. The highest peaks of fluctuations are in the region from 2 to 8 Hz. This value corresponds to the frequency interval of fluctuations of airflow from SEEF, as shown in Fig. 8.

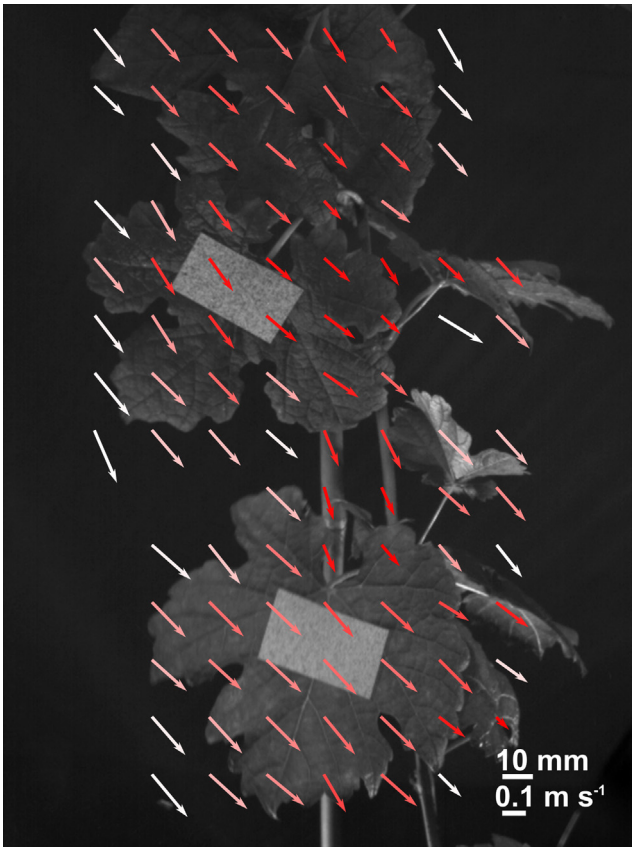

Fig. 10 – Sample average RMS velocity vectors. The location of water sensitive papers can also be seen.

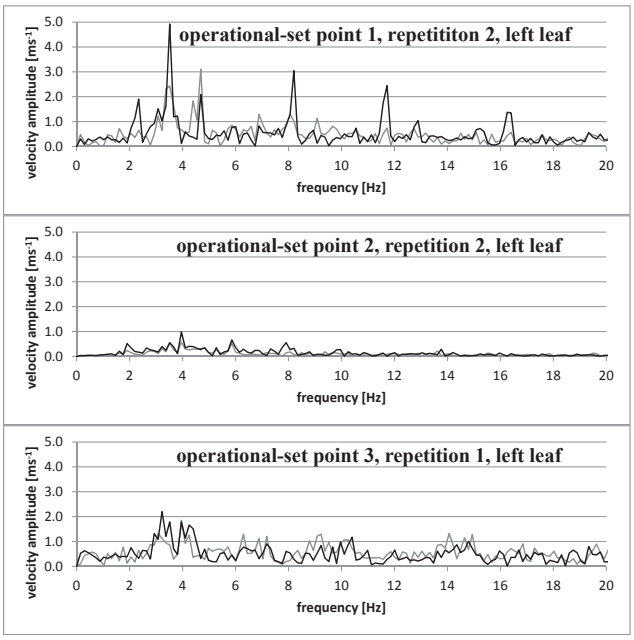

Fig. 11 – Frequency analysis of fluctuation of leaves. Frequency was calculated in selected point. Darker line relates to the horizontal component of velocity and the lighter line to vertical component of velocity.

Velocity was only measured in positions where the plant was present. However, plants were not present at every location for the complete sequence. Such situations occur at the edges of plant. In these positions the RMS velocity is shown in white for the hypothetical case of only one successfully calculated velocity in the sequence. Positions, where plant was present in all image pairs in the sequence, and velocity was successfully calculated, are shown in dark red. All other positions have colours between white and red, depending on the proportion of successfully calculated velocities. Of the many positions where velocity was successfully calculated only in few cases were on the edges of plants. Here RMS velocity is usually very high, as can be seen in Fig. 10.

5. Discussion

Our understanding of precision spraying with the SEEF is the following. The requirement for precision spraying requires a controlled airflow without noteworthy flow fluctuations (in the form of large coherent structures like vortices); otherwise, the airflow fluctuations (high flow turbulence levels) disturb the airflow and prevent precise delivery of the spray. Due to the limited size of the sprayed area the focus is on the movement of single leaves instead of branches. At the location of a targeted leaf, the airflow from a SEEF acts on the leaf with a constant force which moves the leaf from its

equilibrium position to an extreme point, causing bending. Many spray droplet impacts occur on the front of the leaf with very few occurring at the back of the leaf (see Table 2). This situation changes only slightly when airflow pulsations are introduced. The airflow acts on the leaf with an intermittent force, but the force direction and size remain essentially the same. In a very simplified view, the leaf is excited by an intermittent force and it fluctuates from its equilibrium point to both maxima. However, as results in Table 2 show, spray reaching the back of the leaf side is still limited. We believe that the very limited spray reaching the back of the leaves with the SEEF is due to the two factors: (1) the absence of large coherent structures within the spraying airflow carrying spray around plant leaves and (2) the small size of the SEEF not providing large coherent flow structures. The situation is, however, different with the large conventional orchard and vineyard sprayers currently on the market which are able to transport spray around leaves and provide large velocity fluctuation in leaves.

6. Conclusions

The SEEF effector was evaluated for a close range precision spraying process in vineyards. It was found to achieve air flow velocities up to 10 m s^{-1} at distance 0.3 m within diameter around 150 mm. The SEEF was equipped with rotating airflow screen which induced discrete frequency peaks of velocity fluctuations. Measurement of natural frequencies of displacement of leaves in the airflow showed that leaves fluctuate with discrete frequencies. Spraying of front side of leaves surfaces was good, while spraying of back side surfaces should be further improved. Results point to an important drawback of future robotic high precision spraying applications. Such future robotic high precision spraying applications will require positioning of spraying arms and the spraying of disease foci in bush and tree crops from both sides of the plantation row.

Acknowledgement

This work was funded by the European Commission in the 7th Framework Programme (CROPS GA no 246252).

REFERENCES

Andújar, D., Weis, M., & Gerhards, R. (2012). An ultrasonic system for weed detection in cereal crops. *Sensors, 12*(12), 17343–17357.

Ash, G. (2000). Downy mildew of grape, 2000. *The Plant Health Instructor*. http://dx.doi.org/10.1094/PHI-I-2000-1112-01. Updated 2005.

Bontsema, J., Hemming, J., Pekkeriet, E., Saeys, W., Edan, Y., Shapiro, A., et al. (2014). CROPS: high tech agricultural robots. In *International Conference of Agricultural Engineering, Zurich*.

Bruun, H. H. (1995). *Hot-wire anemometry - Principles and signal analysis*. New York: Oxford University Press.

Cunha, M., Carvalho, C., & Marcal, A. R. S. (2012). Assessing the ability of image processing software to analyse spray quality on water-sensitive papers used as artificial targets. *Biosystems Engineering, 111*(1), 11–23.

Cunha, J. P., Chueca, P., Garcerà, C., & Moltò, E. (2012). Risk assessment of pesticide spray drift from citrus applications with air-blast sprayers in Spain. *Crop Protection, 42*, 116–123.

Dekeyser, D., Duga, A. T., Verboven, P., Endalew, A. M., Hendrickx, N., & Nuyttens, D. (2013). Assessment of orchard sprayers using laboratory experiments and computational fluid dynamics modelling. *Biosystems engineering, 114*(2), 157–169.

Endalew, A. M., Debaer, C., Rutten, N., Vercammen, J., Delele, M. A., Ramon, H., Nicolaï, B. M., & Verboven, P. (2010). A new integrated CFD modelling approach towards air-assisted orchard spraying – Part II: Validation for different sprayer types. *Computers and Electronics in Agriculture, 71*(2), 137–147.

Esau, T. J., Zaman, Q. U., Chang, Y. K., Schumann, A. W., Percival, D. C., & Farooque, A. A. (2014). Spot-application of fungicide for wild blueberry using an automated prototype variable rate sprayer. *Precision Agriculture, 15*(2), 147–161.

Jong, F. M. W., Snoo, G. R., & van de Zande, J. C. (2008). Estimated nationwide effects of pesticide spray drift on terrestrial habitats in the Netherlands. *Journal of Environmental Management, 86*, 721–730.

Jørgensen, F. E. (2002). How to measure turbulence with hot-wire anemometers - A practical guide. *Dantec Dynamics*.

Khot, L. R., Ehsani, R., Albrigo, G., Larbi, P. A., Landers, A., Campoy, J., et al. (2012). Air-assisted sprayer adapted for precision horticulture: Spray patterns and deposition assessments in small-sized citrus canopies. *Biosystems Engineering, 113*(1), 76–85.

Mulla, D. J. (2013). Twenty five years of remote sensing in precision agriculture: key advances and remaining knowledge gaps. *Biosystems Engineering, 114*(4), 358–371.

Oberti, R., Marchi, M., Tirelli, P., Calcante, A., Iriti, M., & Borghese, N. A. (2014). Automatic detection of powdery mildew on grapevine leaves by image analysis: optimal view angle to increase the sensitivity. *Computers and Electronics in Agriculture, 104*, 1–8.

Oberti, R., Marchi, M., Tirelli, P., Calcante, A., Iriti, M., Hočevar, M., et al. (2014). Selective precision spraying of grapevine's diseases by crops robot platforms, CROPS: High tech agricultural robots. In *International Conference of Agricultural Engineering, Zurich*.

Oerke, E. C., & Dehne, H. W. (2004). Safeguarding production-losses in major crops and the role of crop protection. *Crop Protection, 23*(4), 275–285.

Otto, S., Mori, N., Fornasiero, D., Veres, A., Tirello, P., Pozzebon, A., et al. (2013). Insecticide drift and its effect on Kampimodromus aberrans (Oudemans) in an Italian vineyard-hedgerow system. *Biosystems Engineering, 116*, 447–456.

Porras-Soriano, A., Porras-Piedra, A., & Soriano-Martn, M. L. (2005). Quality of fungicide application on trellised grapevines by a sprayer prototype. *Agronomy for Sustainable Development, 25*(2), 201–204. Springer Verlag (Germany).

Pujol, D., Casamitjana, X., Serra, T., & Colomer, J. (2013). Canopy-scale turbulence under oscillatory flow. *Continental Shelf Research, 66*, 9–18.

Sánchez-Hermosilla, J., Rincón, V. J., Páez, F., & Fernández, M. (2012). Comparative spray deposits by manually pulled trolley sprayer and a spray gun in greenhouse tomato crops. *Crop Protection, 1*(1), 119–124.

Syngenta. (2002). *Water-sensitive paper for monitoring spray distributions*. Basel: Syngenta Crop Protection AG.

West, J. S., Bravo, C., Oberti, R., Lemaire, D., Moshou, D., & McCartney, H. A. (2003). The potential of optical canopy

measurement for targeted control of field crop diseases. *Annual Review of Phytopathology, 41*(1), 593–614.
Zamana, Q. U., Esaua, T. J., Schumannb, A. W., Percivalc, D. C., Changa, Y. K., Reada, S. M., et al. (2011). Development of prototype automated variable rate sprayer for real-time spotapplication of agrochemicals in wild blueberry fields. *Computers and Electronics in Agriculture, 76*(2), 175–182.